Nanoductility induced brittle fracture in shocked high performance ceramics

Paulo S. Branicio,[1,a)] Rajiv K. Kalia,[2] Aiichiro Nakano,[2] and Priya Vashishta[2]
[1]*Materials Theory and Simulation Laboratory, Institute of High Performance Computing, 1 Fusionopolis Way 16-16, Connexis, Singapore 138632*
[2]*Collaboratory for Advanced Computing and Simulations, Department of Chemical Engineering and Materials Science, Department of Physics and Astronomy, and Department of Computer Science, University of Southern California, Los Angeles, California 90089, USA*

(Received 30 May 2010; accepted 9 July 2010; published online 13 September 2010)

Nanoductility induced crack nucleation mechanism mediated by a single dislocation core is revealed in a 300 million-atom molecular dynamics simulation of shocked silicon carbide ceramic. The atomistic damage mechanism involves dynamic transitions between clearly delineated regimes—from shock-induced structural transformation to plastic deformation to brittle fracture. Such atomistic understanding may help in the design of nanocrack suppression strategies to realize predictive modeling of complex damage processes in high-performance ceramics. © *2010 American Institute of Physics*. [doi:10.1063/1.3478003]

Advances in experimental methods, such as *in situ* microcompression and atomic force microscopy, have provided new insights into the role of nanoplasticity in known brittle materials.[1,2] In contrast with bulk materials, experiments have shown surprising existence of ductility at the nanoscale, e.g., metallic glass nanopillars may behave similar to ductile metals,[2] and nanovoid coalescence was shown to play an important role in the ductile fracture mechanism in silica.[3,4] Similarly, nanoductility has been shown to play a crucial role in the damage initiation in high-strength ceramics under high-velocity impact.[5,6] Nanoplasticity could be a key ingredient to understand and improve high performance ceramics such as AlN, Al_2O_3,[7] SiC,[8–10] and their composites that are known for their outstanding mechanical properties and make these materials ideal for structural applications involving high temperature and pressure.[11,12] It is essential to clarify the role of nanoplasticity and to evaluate intrinsic mechanisms of damage leading to fracture at extreme conditions of temperature and pressure. Shock induced damage by projectile impact is an essential tool in this regard, since it provides an ideal environment of extreme conditions of high gradients of pressure, temperature, and density.

In this letter, we describe an ultra-large-scale molecular dynamics simulation of projectile impact on SiC. We use a many-body interatomic potential,[15,16] for SiC[17] reflecting first-principles information.[13,14] In the simulation a 3C–SiC target is impacted at 15 km/s and the atomic trajectories are calculated as a function of time allowing an accurate description of the spontaneous shock-induced damage dynamics. The zinc blende single crystal 3C–SiC target containing 302 million atoms has dimensions $160 \times 158 \times 124$ nm^3 in the x, y, and z directions. The z-axis, parallel to the [111] direction of the zinc blende crystal, is chosen as the impact direction. Periodic boundary conditions are imposed in the x and y directions, parallel to the $[\bar{2}11]$ and $[0\bar{1}1]$ directions. In the z direction the target has two free surfaces; see Fig. 1(a). The projectile is a hexagonal cylinder, 15 nm wide and 30 nm long, with 563 000 atoms. The projectile is five times stiffer and its atoms are five times heavier than those of the target. The interatomic potential between the target and projectile atoms is purely repulsive. A Langevin damping of the shock waves is applied to the boundaries along the x and y directions to avoid reflection of the waves. Defects in the system are dynamically data mined during the whole simulation using shortest path rings selection rules in a highly efficient implementation.[18] Local stresses are calculated using the atomic Virial averaged spherically around each atomic position.[19]

During the first picosecond of penetration the projectile releases a large amount of kinetic energy into the target [Fig. 1(a)], which results in a high local energy density. The large gradients of pressure and temperature causes localized melting and vaporization,[20,21] and creates a strong shock wave with peak pressure of 150 GPa and speed of up to 24 km/s. During the shock propagation into the target, wherever the

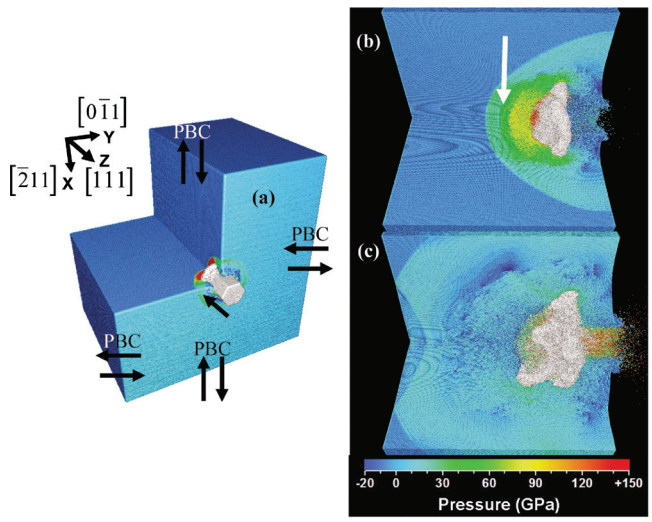

FIG. 1. (Color) Shock evolution during hypervelocity impact on SiC ceramics. (a) Shock generation at 1.05 ps. Projectile atoms are shown in grey. Target atoms colors follow the local pressure. (b) Splitting of shock wave (see white arrow) into an elastic wave (light green) and a structural phase transformation wave (yellow/dark green) at 5.17 ps. (c) Reflection of compressive wave at the back surface generates a tensile release wave at 10.35 ps.

a)Author to whom correspondence should be addressed. Electronic mail: branicio@ihpc.a-star.edu.sg.

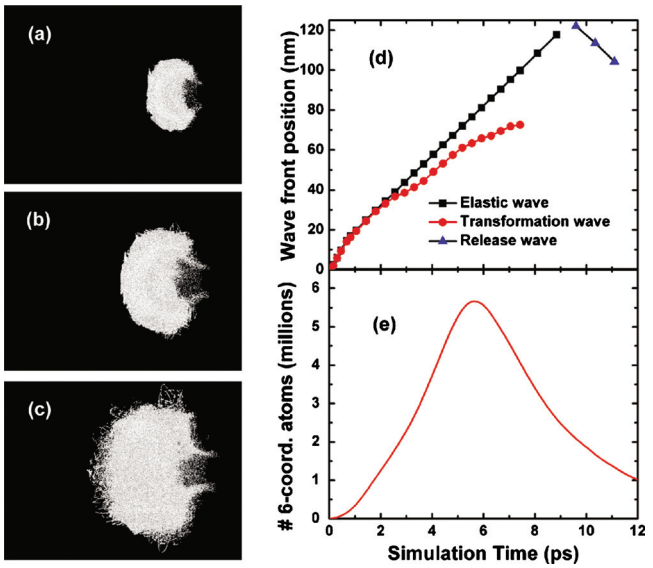

FIG. 2. (Color) Shock-induced structural phase transformation. (a) Cluster of 6 coordinated atoms at 3 ps, (b) at 5.5 ps, and (c) at 9 ps. (d) Evolution of shock fronts with time. (e) Number of 6 coordinated atoms with time.

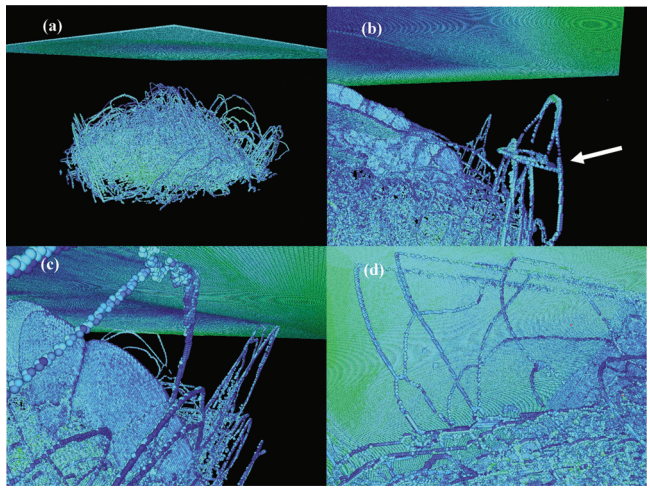

FIG. 3. (Color) Shock-induced plasticity in SiC. Only atoms in the left half system of Figs. 1(b) and 1(c) are shown here, with the back target surface on top. Also, only atoms forming defects, i.e., dislocations, surfaces and crack surfaces are shown. (a) Dislocation loops emitted from the interface of the transformed and untransformed phases at 11.1 ps. (b) Detail of a dislocation dissociation and multiplication (see white arrow) at 14.4 ps. (c) Dislocation lines propagating in {111} slip planes reaching the back surface at 17.7 ps (d) Dislocation structures connected with the back surface at 31.2 ps.

pressure of the shock front reaches a critical value of 89 GPa, the material undergoes a structural phase transformation (SPT) from the fourfold-coordinated zinc blende structure to the sixfold-coordinated rock salt structure. This SPT accompanies the shock wave as long as the pressure is above the critical value. In about 7.5 ps, the transformation wave slows down significantly and the SPT stops when the local pressure drops below the threshold value of 89 GPa. The elastic component of the shock wave continues to travel through the system at an average speed of 12.5 km/s, which is close to the longitudinal sound speeds of 3C–SiC.[17,22] The shock wave split is evident in Fig. 1(b) where it is indicated by the white arrow. The elastic wave continues to propagate until it reaches the back surface and generates a release wave back into the system; see Fig. 1(c).

Figures 2(a)–2(c) show that the SPT wave has an almost spherical shape with a rough surface formed by the nucleation of rock salt clusters with a heterogeneous grain structure of different sizes and orientations. At about 9 ps the decreasing stress at the shock front decrease the rate of transformation and the SPT shock front starts to become rough and undefined as shown in Fig. 2(c). Figure 2(d) shows that from 5.5 ps the split in the shock fronts increases until the SPT wave virtually stops. The evolution curve of the number of 6 coordinated atoms shown in Fig. 2(e) indicates a maximum at about 5.5 ps. After that the reverse transformation occurs at a fast rate as the local pressure drops with the dissipation of the shock wave energy. With the attenuation of the shock pressure, the SPT stalls and the generation of plastic deformation becomes the dominant mechanism of damage. In the central region surrounding the impact path high levels of shear stress are generated and they are released by the generation of dislocations. The results indicate that initially the plastic zone is rooted at the zinc blende-rock salt interface, which is a favorable spot for stress concentration and defect nucleation. When the hydrostatic pressure is not high enough to drive the SPT, the interface becomes rough and the high local shear stress causes spontaneous emission of dislocations into the zinc blende phase. Figure 3(a) illustrates the emission of dislocations from this region at 11.1 ps.

The zinc blende cubic structure of SiC has the {111} family of planes as the preferred, lowest energy, set of planes for dislocation gliding. The distribution of high levels of shear stress around the shock front generates dislocation lines on all {111} planes. While the shear stress is not aligned to any {111} glide plane the component of the shear stress along several of them is enough to trigger the generation and propagation of dislocations which glide away from the central region to adjacent regions of the system while propagating to the back surface; see Figs. 3(a)–3(c). An estimation of the shear stress levels in the central region along the impact z direction by $\tau=0.5[\sigma_{zz}-0.5(\sigma_{xx}+\sigma_{yy})]$, gives values up to 45 GPa. The high shear stress and the rough surface of the interface of rock salt and zinc blende structures favor the emission of a large number of dislocations, forming a complex configuration. As dislocations are emitted they propagate until they reach the back surface, leaving surface steps; see Figs. 3(c) and 3(d).

Dislocations show a rich dynamics in the propagation to the back surface. The flow of atoms in the central region of the target creates shear stress that favors the glide of dislocations in the z direction to the back surface of the system. As this shear stress is not aligned with {111} planes, several dislocation dynamic processes have a propitious environment, such as dislocations climb, cross slip, and multiplication of dislocations. All these processes are active and enhanced by the overlap of compressive and tensile shock waves. Dissociation, multiplication, and cross slip of dislocations are illustrated in Fig. 3(b). In the process of cross slip the results show the formation of dislocation locks and structural debris; see Fig. 3(d).

When the compressive shock wave reaches the back surface, it generates a tensile release wave back into the target, which reduces the local hydrostatic pressure to negative values, locally reaching up to -20 GPa. That causes the spontaneous emission of cracks from the plastic deformed region. Our analyses indicate that when the release wave reaches the

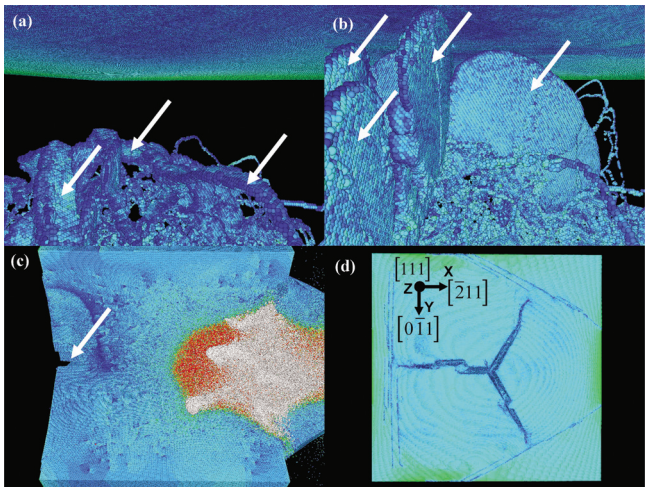

FIG. 4. (Color) Nucleation and growth of brittle cracks from dislocations in shocked SiC. (a) White arrows indicate brittle cracks nucleating directly from dislocation lines at 13.05 ps. (b) Cracks cleaving {110} planes of the zinc blende crystal in the direction of the back surface. (c) Cracked configuration at 27 ps. (d) Cracked back surface at 31.2 ps.

dislocation structures, as illustrated in Fig. 3(a), it causes the immediate emission of microcracks from dislocation line cores; see Fig. 4(a). The process occurs in all {110} planes, which are the lowest surface energy, preferred planes for crack cleavage.[23] This process of microcrack emission from single dislocation cores is one of the most striking features of this work, since it is the first time that it has been numerically demonstrated as a possible mode of microcrack nucleation. While the system simulated is orders of magnitude smaller than a real projectile impact experiment there is vast experimental evidence that the release wave have a very active role in the damage nucleation and in fracture generation, see Branicio *et al.*[6] and references within.

Nucleated microcracks grow cleaving initially all the six planes of the {110} family. As the tensile stress is released, microcracks on planes {0$\bar{1}$1}, {10$\bar{1}$}, and {$\bar{1}$10}, growing in the [111] direction to the back surface, merge with other microcracks forming larger cracks cleaving extensive planes of the zinc blende crystal until they reach the back surface; see Fig. 4(b). The growth of the cracks is not shielded by the emission of dislocations and it results in clean cleavage surfaces. Because of confinement the crack partially heals as the tensile stress is relaxed. Figure 4(c) shows the system in a 3/4 configuration at 27 ps showing the whole fractured system. Figure 4(d) shows the cracked back surface of the target at 31.2 ps with three major cracks on {0$\bar{1}$1}, {10$\bar{1}$}, and {$\bar{1}$10} planes.

The role of plastic structures in the process of microcrack nucleation in ceramics is overlooked in the literature. In brittle high-strength ceramics, plasticity is restricted and failure generally occurs with little plastic deformation, except at high temperatures or high stresses,[24,25] where plasticity is favored. Because of this restricted plasticity, the role of plastic structures in the damage response of ceramics at extreme conditions of stress is rarely discussed in the literature. Here we demonstrate that plastic structures may have a complex dynamics in ceramics and have a central role in the failure by direct microcrack nucleation. In the literature only Fu, Evans, and Kriven,[26] to the best of our knowledge, have suggested that single dislocation line cores can in principle be a source for stress concentration and microcrack nucleation. In their work, however, the microcrack initiation was analyzed only in twinned ZrO_2 ceramics. Our results demonstrated for the first time that micro crack initiation from dislocation lines is a plausible mechanism also in monolithic SiC ceramics. This behavior is very surprising because the common mechanisms for microcrack nucleation, i.e., from microvoids or dislocation coalescence, are both active in AlN ceramics.[5] Several details related to the results presented here would require deeper analysis or new studies. In particular the stress and temperature conditions necessary to trigger dislocation dynamics and its role in the generation of microcracks in ceramics deserve further studies. The atomistic details from this study concerning the SPT and plasticity dynamics and the direct link to brittle fracture may be incorporated into continuum simulations and enable predictive modeling of damage processes in brittle ceramics.

Work supported by the Materials Sciences and Engineering Division and the Center for Energy Nanoscience, an Energy Frontier Research Center, of the DOE-Office of Basic Energy Sciences, the SciDAC program of the DOE-Office of Advanced Computing Research, NSF-PetaApps and NSF-EMT.

[1] D. Kiener, C. Motz, and G. Dehm, Mater. Sci. Eng., A **505**, 79 (2009).
[2] D. C. Jang and J. R. Greer, Nature Mater. **9**, 215 (2010).
[3] F. Célarié, S. Prades, D. Bonamy, L. Ferrero, E. Bouchaud, C. Guillot, and C. Marlière, Phys. Rev. Lett. **90**, 075504 (2003).
[4] T. Campbell, R. K. Kalia, A. Nakano, F. Shimojo, K. Tsuruta, P. Vashishta, and S. Ogata, Phys. Rev. Lett. **82**, 4018 (1999).
[5] P. S. Branicio, R. K. Kalia, A. Nakano, and P. Vashishta, Phys. Rev. Lett. **96**, 065502 (2006).
[6] P. S. Branicio, R. K. Kalia, A. Nakano, P. Vashishta, F. Shimojo, and J. P. Rino, J. Mech. Phys. Solids **56**, 1955 (2008).
[7] C. Zhang, R. K. Kalia, A. Nakano, P. Vashishta, and P. S. Branicio, J. Appl. Phys. **103**, 083508 (2008).
[8] I. Szlufarska, R. K. Kalia, A. Nakano, and P. Vashishta, Appl. Phys. Lett. **85**, 378 (2004).
[9] I. Szlufarska, A. Nakano, and P. Vashishta, Science **309**, 911 (2005).
[10] H. P. Chen, R. K. Kalia, A. Nakano, P. Vashishta, and I. Szlufarska, J. Appl. Phys. **102**, 063514 (2007).
[11] M. E. Levinshteæin, S. L. Rumyantsev, and M. Shur, *Properties of Advanced Semiconductor Materials: GaN, AlN, InN, BN, SiC, SiGe* (Wiley, New York, 2001).
[12] A. Pechenik, R. K. Kalia, and P. Vashishta, *Computer-aided Design of High-temperature Materials* (Oxford University Press, New York, 1999).
[13] S. Yip, *Handbook of Materials Modeling* (Springer, Berlin, 2005).
[14] C. Y. Fong, M. C. Qian, J. E. Pask, L. H. Yang, and S. Dag, Appl. Phys. Lett. **84**, 239 (2004).
[15] P. Vashishta, R. K. Kalia, A. Nakano, and J. P. Rino, J. Appl. Phys. **103**, 083504 (2008).
[16] P. Vashishta, R. K. Kalia, A. Nakano, and J. P. Rino, J. Appl. Phys. **105**, 059901 (2009).
[17] P. Vashishta, R. K. Kalia, A. Nakano, and J. P. Rino, J. Appl. Phys. **101**, 103515 (2007).
[18] C. Zhang, B. Bansal, P. S. Branicio, R. K. Kalia, A. Nakano, A. Sharma, and P. Vashishta, Comput. Phys. Commun. **175**, 339 (2006).
[19] P. S. Branicio and D. J. Srolovitz, J. Comput. Phys. **228**, 8467 (2009).
[20] B. L. Holian, Phys. Rev. A **37**, 2562 (1988).
[21] A. B. Belonoshko, Science **275**, 955 (1997).
[22] M. Prikhodko, M. S. Miao, and W. R. L. Lambrecht, Phys. Rev. B **66**, 125201 (2002).
[23] H. Kikuchi, R. K. Kalia, A. Nakano, P. Vashishta, P. S. Branicio, and F. Shimojo, J. Appl. Phys. **98**, 103524 (2005).
[24] M. Azzaz, J. P. Michel, V. Feregotto, and A. George, Mater. Sci. Eng., B **71**, 30 (2000).
[25] X. J. Ning and P. Pirouz, J. Mater. Res. **11**, 884 (1996).
[26] Y. Fu, A. G. Evans, and W. M. Kriven, J. Am. Ceram. Soc. **67**, 626 (1984).